Available online at www.sciencedirect.com
SCIENCE DIRECT®
Journal of Sound and Vibration 275 (2004) 249–265
JOURNAL OF SOUND AND VIBRATION
www.elsevier.com/locate/jsvi

An investigation of the flow-induced sound and vibration of viscoelastically supported rectangular plates: experiments and model verification

J. Park[1], L. Mongeau*, T. Siegmund

Ray W. Herrick Laboratories, Purdue University, 140 S. Intramural Drive, West Lafayette, IN 47907-2031, USA

Received 25 June 2002; accepted 18 June 2003

Abstract

Experiments were performed in order to investigate the vibration response and the sound radiation of a viscoelastically supported, rectangular aluminum plate excited by turbulent flows. The primary goal of this investigation was to assess the influence of seal mechanical properties and geometries on the noise generated from side-glass windows in road vehicles. The modal properties of seal-supported plates were determined in the experiments. Measurements of surface wall pressure fields were performed using small-diameter condenser microphones. Two different types of turbulent flow excitation and two different types of sealing systems used as supports of the plate were investigated. The measured results were in good agreement with predictions from an analytical model described in previous publications. The study confirms the postulated mechanism for vibration energy dissipation at the boundary, the reduction in amplitude of the plate vibration at resonance, and the reduction of the associated radiated sound.

1. Introduction

Aerodynamic noise is an important source of interior noise in road vehicles [1]. The front windows are located near driver and front passenger ears, and the sound radiated from the front window panels is thus considered a primary source of aerodynamic broadband noise [2,3], although other flow-excited structural elements are also believed to contribute [4]. The study of aerodynamic noise generated from flow-excited structures involves the investigation of the wall

*Corresponding author. Tel.: +1-765-494-9342; fax: +1-765-494-0787.
E-mail address: mongeau@ecn.purdue.edu (L. Mongeau).
[1] Present address: National Research Council, NASA Langley Research Center, Hampton, VA 23681-2199, USA.

0022-460X/$ - see front matter © 2003 Elsevier Ltd. All rights reserved.
doi:10.1016/j.jsv.2003.06.017

pressure fluctuations on the structure, the structural vibrations excited by the surface pressure field, and finally the sound radiated from the vibration of the structure. The direct radiation of sound from the unsteady pressure field will be neglected in the following.

The dynamic pressure fluctuations generated by the interaction of unsteady or turbulent flows with flexible structures have received a considerable amount of attention [5]. Velocity fluctuations within the turbulent boundary layers contribute to the wall pressures on the structure. Due to the complex nature of the turbulent flow, statistical descriptions of the wall pressure fields are widely used.

When the surfaces of the structure are irregular, the turbulence intensity of the grazing flows is significantly increased relative to flows grazing over smooth and flat surfaces. Farabee and Casarella [6,7] conducted experiments for two different types of irregularities: backward facing and forward facing step flows in a low noise wind tunnel. The flow reattachment zone was revealed as a source of large amplitude, low-frequency fluctuations.

Strawderman and Brand [8] used the cross-power spectral density of wall pressure fluctuations to study the structural response of simply supported rectangular plates. The Corcos wall pressure model [9] was used. The plate response was calculated using a modal expansion method. Han et al. [10] measured the wall pressure spectrum over a flat plate in a quiet wind tunnel facility and used the energy flow analysis (EFA) method to predict the flow-induced vibration response. The Corcos model [9] was used for the regions under separated or reattached flows. The EFA method was found to yield approximate predictions of the frequency-averaged transverse velocity response of flow-excited plates at high frequencies.

Until now, there have been few investigations on flow-induced vibrations of plates with arbitrary boundary conditions. Most studies of flow-induced vibrations of plates have been devoted to simply supported, clamped, or free rectangular plates because of their practical importance. The influence of the dynamic mechanical properties of the elements supporting the plate was investigated analytically in Ref. [11]. The Rayleigh–Ritz method was used using beam functions as the trial functions. Theoretical methods to calculate the optimal support stiffness were presented in Ref. [12]. It was found that the modal response is strongly regulated by the energy dissipation at the edges, which determined the amplitudes of the spatially averaged vibration response and the radiated sound power.

In this study, the physical parameters influencing the vehicle interior noise are measured in a controlled laboratory set-up to investigate the noise generated from flow-induced vibration of a viscoelastically supported plate. Especially the effects of viscoelastic supports are determined by experiments. The measurement results verified the prediction of an analytical model presented in a previous publication by the authors [11,12].

Specific procedures are listed in the following. Experimental modal analysis tests were conducted to accurately measure the modal parameters of the seal-supported plate. The measured modal parameters were used to estimate the mechanical properties of the viscoelastic seal supports. The statistical characteristics (assumed stationary and homogeneous) of the wall pressure field in the wind tunnel facility were measured. The pressure field was expressed by a cross-correlation function, assuming exponential decay with position and time of frozen flow structures convected with the mean flow. The sound power radiated from flow-induced vibration of the rectangular plate was measured. Finally, the comparison of the results with analytical model enhances the understanding of the wind noise generating mechanisms.

2. Experimental apparatus

Experiments were performed using a custom-built test fixture installed in a low-speed wind tunnel (open-circuit type), as depicted in Fig. 1. A rectangular, flat aluminum plate supported on all four edges by a glass-run sealing system was mounted on a rigid aluminum frame connected to a rectangular, acoustically treated enclosure. The aluminum plate was used to approximate a glass window plate. The plate was 47 cm long, 37 cm wide and 0.34 cm thick. The frame was flush with the wind tunnel test section floor and structurally isolated from the vibration of the wind tunnel walls using a foamed rubber and silicone. The wind tunnel included many vibration isolation and muffling devices. These minimized the acoustic noise in the wind tunnel test section, the turbulence level of the inflow at the wind tunnel inlet, and the mechanical vibrations of the test section walls. The rectangular test section measured $61 \times 46 \times 152\,\mathrm{cm}^3$. The maximum obtainable flow velocity was 50.9 m/s with 1% spanwise uniformity. More details of the design, construction, and validation of the wind tunnel are given in Ref. [13].

Test fixtures for two different seal designs (a flange-mounted seal and a channel-mounted seal) were used, as shown in Fig. 2. Both seals were made of foamed rubber and plain rubber compounds, with a low-friction coating. The seals are representative of many seals currently used in cars and trucks. Efforts were made to ensure a uniform support around all four edges of the plates. The corners were cut at a 45° angle and sealed using silicone and vacuum grease.

The vibration response of the plate was measured using a scanning Polytec laser vibrometer (Fig. 3), equipped with a controller processor model OFV-3000, a laser beam shutter model OFV-302, and a scanning controller system model OFV-042. The laser vibrometer was suspended vertically, 1.5 m above the wind tunnel test section ceiling, which was made of 1.25 cm thick Plexiglas for optical access. The plate velocity response was measured at 80 equally spaced points over the plate surface. To maximize the intensity of the reflected laser beam, the plate was coated with a mixture of paint and glass particles. The frequency range was limited to 0–1.4 kHz by the relatively low excitation levels at high frequencies, the limited dynamic range (or amplitude resolution) of the laser, and the reflections of the laser beam off the wind tunnel ceiling Plexiglas panel. The sound radiated from the plate was measured using a 13 mm condenser microphone

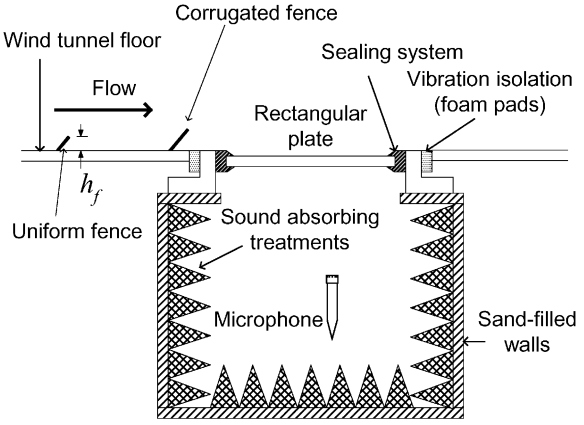

Fig. 1. Experimental apparatus.

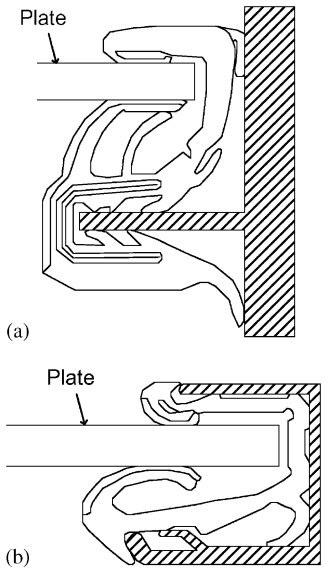

Fig. 2. Cross-section of sealing systems used in the experiments: (a) flange-mounted sealing system, (b) channel-mounted sealing system.

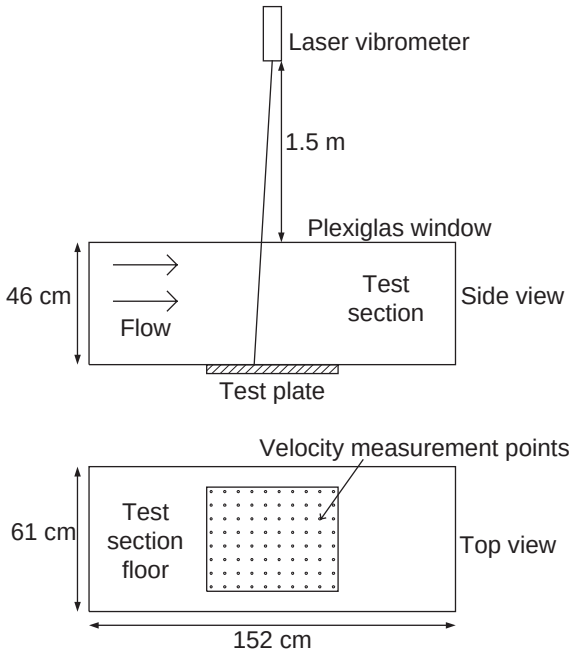

Fig. 3. Schematic of the wind tunnel test section, the laser vibrometer and the velocity measurement locations on the plate.

(Brüel & Kjær Type 4189) located inside the enclosure. A four-channel data acquisition system was used to acquire and process the data.

Measurements of the frame vibrations were performed and revealed that the top of the sound receiving enclosure was not perfectly rigid. This resulted in a low-frequency resonance of the frame/plate assembly in the frequency range between 30 and 70 Hz. This low-frequency resonance, which stands out in all the experimental results, involves the rigid body translation of both the frame and the plate, and almost no relative displacement between the frame and the plate. Therefore, this low-frequency resonance was not considered as a genuine mode of the plate. Since the natural frequencies of this low-frequency resonance were smaller than the fundamental frequency of the viscoelastically supported plate, the low-frequency resonance was neglected in the following analysis.

3. Turbulent wall pressure measurements

The Corcos model was used to obtain a statistical description of the wall pressure field. The advantage of the Corcos model is its simplicity compared to other wall pressure models. The cross-power spectral density between the pressures measured at two points on the plate is expressed as

$$\hat{G}_{pp}(\xi_x, \xi_y, \omega) = \Phi_p(\omega) e^{-\gamma_x |\omega \xi_x / U_c|} e^{-\gamma_y |\omega \xi_y / U_c|} e^{-i\omega \xi_x / U_c}, \quad (1)$$

where U_c is the flow convection speed, Φ_p is the wall pressure spectral density, ξ_x and ξ_y are the separation distances, γ_x and γ_y are the decay rates, and $i = \sqrt{-1}$.

To determine the parameters of the Corcos model, the wall pressure spectra over the plate were measured. The microphone array consisted of five condenser microphones (Knowles Electronics, Type EK-3024) mounted flush with the wind tunnel floor as shown in Fig. 4. The distance between two adjacent microphones in the microphone array was 12.7 mm. Each microphone had an effective circular sensing diameter of 1.37 mm. The microphones were calibrated by comparison to a 13 mm condenser microphone (Brüel & Kjær Type 4189) using an intensity calibrator (Brüel & Kjær 3541 sound intensity calibrator).

Fences were installed upstream of the test plate in order to increase the surface pressure level (Figs. 1 and 4). The enhanced excitation level increased the sound radiated from the plate into the

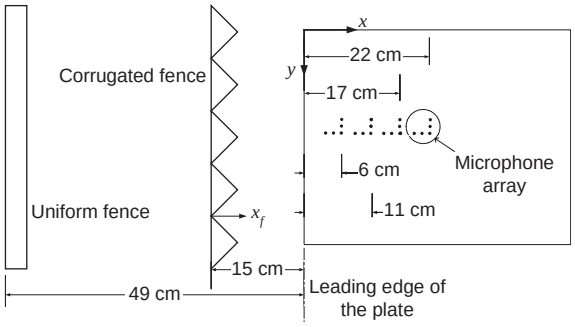

Fig. 4. Fence and microphone array locations.

enclosure relative to other noise sources, including the sound from the operation of the wind tunnel and the structural sound radiating through flanking paths. Two different fences were used: (1) a uniform fence ($h_f = 4.3$ cm) located 49 cm from the leading edge of the plate; and (2) a corrugated fence ($h_f = 8.5$ cm) located 15 cm from the leading edge of the plate. For the uniform fence, the fence location was such that the flow reattachment line was approximately at the leading edge of the plate [10]. Thus, a reattached flow was generated on the plate surface when the uniform fence was installed. The corrugated fence was used to achieve greater pressure in the frequency range between 400 and 1500 Hz, which improved the quality of the laser vibrometer signals. When the corrugated fence was installed, separated and reattached flows co-existed on the plate surface and designated as the separated/reattached flow in the following sections. The convection velocity depends on the frequency, flow speeds, and boundary layer thickness [14]. In this study, the turbulence convection velocity was approximated as $U_c = 0.50U_0$ for the separated/reattached flow and the reattached flow, and $U_c = 0.65U_0$ for the equilibrium flow (a flow with no fence installed) where U_o is the free stream flow speed [10].

3.1. Auto-power spectrum of the wall pressure

Fig. 5 shows the wall pressure spectra measured for different flow speeds and fence types. Non-dimensional pressure and frequency parameters were formed using free-stream flow velocity and the height of the fence. For the equilibrium flow, the measured boundary layer thickness (2.9 mm) reported by Brown and Mongeau [13] was used instead of the fence height. For each fence type, the non-dimensional pressure measured for the different flow speeds collapsed into a single curve. The experimental data show that the wall pressure spectra for the reattached flow are very rich in low frequency energy. Similar trends were observed in the comparison between the equilibrium flow and the separated/reattached flow. The amplitude of the wall pressure spectra at low frequencies was greater by more than 30 dB for the reattached and the reattached/separated flow than that for the equilibrium flow, which is indicative of highly energized, organized turbulent flow.

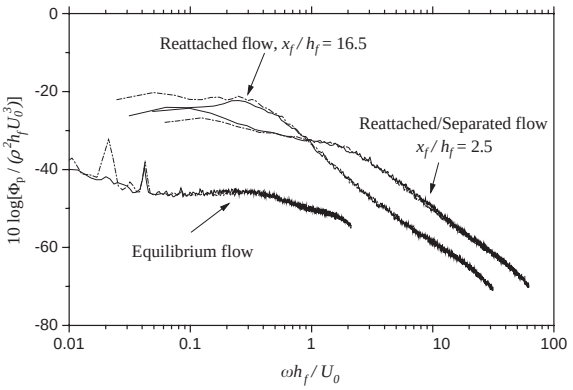

Fig. 5. Wall pressure spectral density scaled on outer flow variables and fence height: ——, $U_0 = 34.4$ m/s; - - - - - -, $U_0 = 43.6$ m/s.

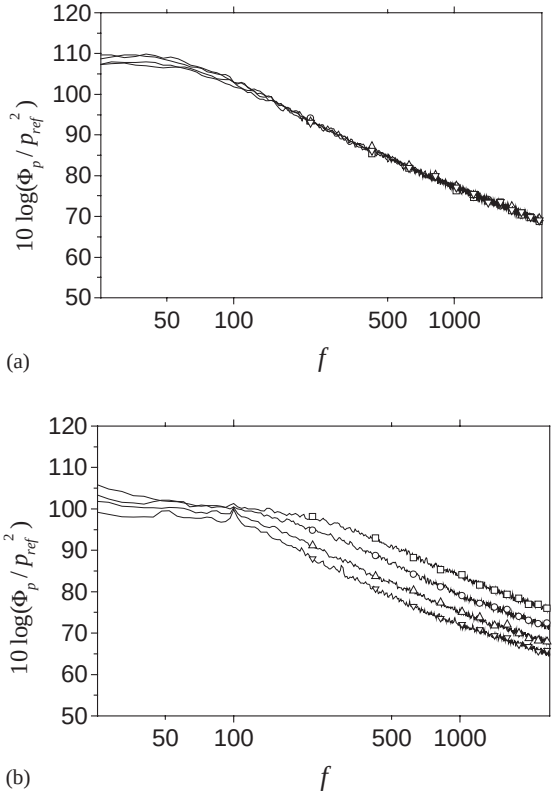

Fig. 6. Wall pressure spectral density measured for two different flows: (a) the reattached flow for x_f/h_f : —□—, 12.8; —○—, 14.0; —△—, 15.3; —▽—, 16.5; (b) the separated/reattached flow for x_f/h_f : —□—, 2.5; —○—, 3.1; —△—, 3.8; —▽—, 4.4.

Fig. 6(a) shows wall pressure spectra measured at four different locations on the plate under the reattached flow. The variation with streamwise position was negligible. In the reattached flow, the flow was more spatially homogeneous compared to the separated/reattached flow. Fig. 6(b) shows the streamwise variation of the measured wall pressure spectra for the separated/reattached flow. More variations were observed compared to those of the reattached flow.

3.2. Coherence variation

Fig. 7 shows the ordinary coherence function between the two wall pressure signals for the two flow velocities and two separation distances in the streamwise direction measured for the equilibrium flow. In agreement with the assumption of the Corcos model, the coherence variation with the non-dimensional parameter, $\omega\xi_x/U_c$, collapsed into an exponential decay curve. The estimated value of the decay rate, γ_x, was 0.14. This decay rate was similar to the values found in the literature [8,10,14] for equilibrium flows.

Figs. 8(a) and (b) show coherence variations in the streamwise and spanwise directions, respectively, measured for the reattached flow at the center of the plate. The coherence variation was in good agreement with the exponential decay functions. The decay rates, γ_x and γ_y, were

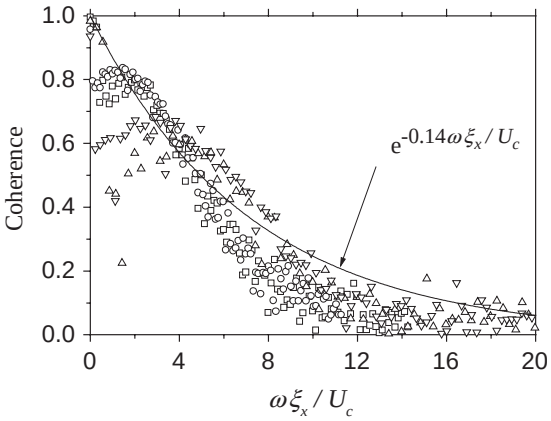

Fig. 7. Streamwise coherence variations with free stream velocities (U_0) and separation distances (values in the parentheses): □, 34.4 m/s (12.7 mm); ○, 34.4 m/s (25.4 mm); △, 43.6 m/s (12.7 mm); ▽, 43.6 m/s (25.4 mm), measured at the center of the plate for the equilibrium flow.

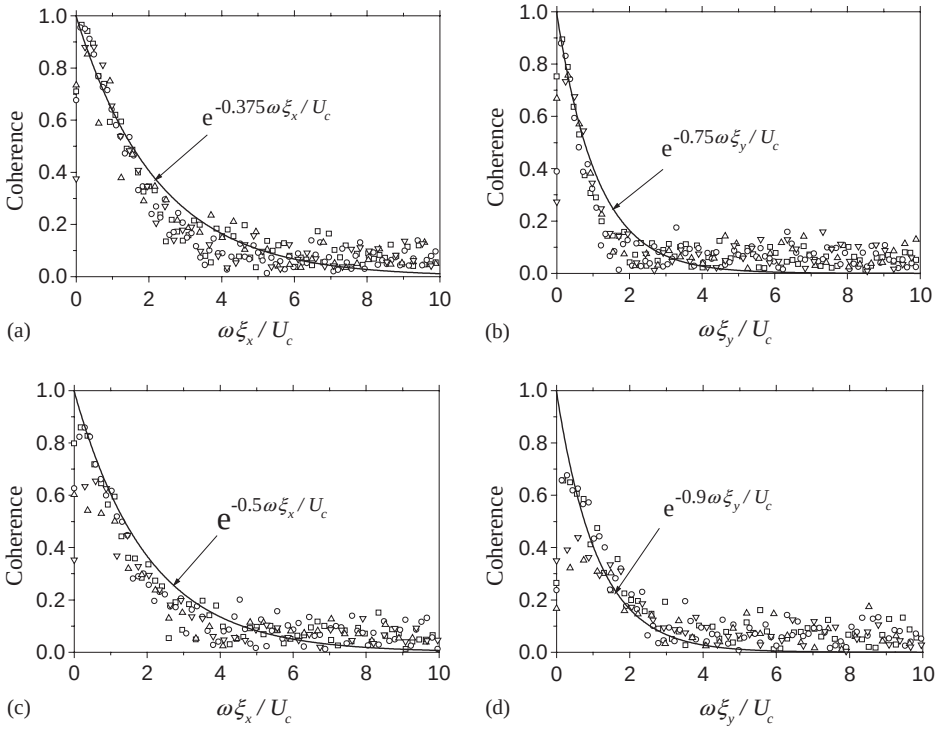

Fig. 8. Coherence variations for two different flow types—reattached flow measured at the center of the plate in (a) the streamwise direction and (b) the spanwise direction, separated/reattached flow measured at the leading edge of the plate in (c) the streamwise direction and (d) the spanwise direction. Free stream velocities (U_0) and separation distances (values in the parentheses): □, 34.4 m/s (12.7 mm); ○, 34.4 m/s (25.4 mm); Δ, 43.6 m/s (12.7 mm); ▽, 43.6 m/s (25.4 mm).

estimated as 0.375 and 0.75, respectively. Figs. 8(c) and (d) show the coherence variations measured for the separated/reattached flow at the leading edge of the plate. The decay rates, γ_x and γ_y, were estimated as 0.50 and 0.90, respectively. The estimated decay rates are much higher than those estimated for the equilibrium flow, which is indicative of the increased turbulence level by the installed fence. Although the measured wall pressure spectra differed significantly between those measured for the reattached flow and the separated/reattached flow (Fig. 5), the decay rates were similar to each other.

4. Experimental modal analysis

Experimental modal analysis test were performed to measure natural frequencies, damping ratios, and mode shapes of the plate. The plate was first tested in its free state and then with the seals and fixtures attached. In order to approximate a free boundary condition, the plate was suspended using a very compliant support (compliant cord). The seal-supported plate was mounted onto the sound-receiving enclosure, which was used for the wind tunnel tests in order to account for possible coupling with low-frequency acoustic cavity modes. Then, the plate surface was subdivided into 80 equally sized square elements. A single-input and single-output method was followed and a roving hammer and a fixed accelerometer were used. The frequency response functions were measured in the frequency range of 0–500 Hz with a resolution of 1.25 Hz, using a ''box-car'' window. Experimental modal analysis was performed using commercially available software (STAR Modal, Spectral Dynamics Inc.).

Figs. 9 and 10 show the measured modal parameters—mode shapes, natural frequencies and damping ratios. For the free plate, Fig. 9, nine modes were identified with natural frequencies in the 0–500 Hz range for the free plate. The damping ratios were less than 1% for all nine modes. Some modes had very similar natural frequencies. When the plate was supported by the sealing

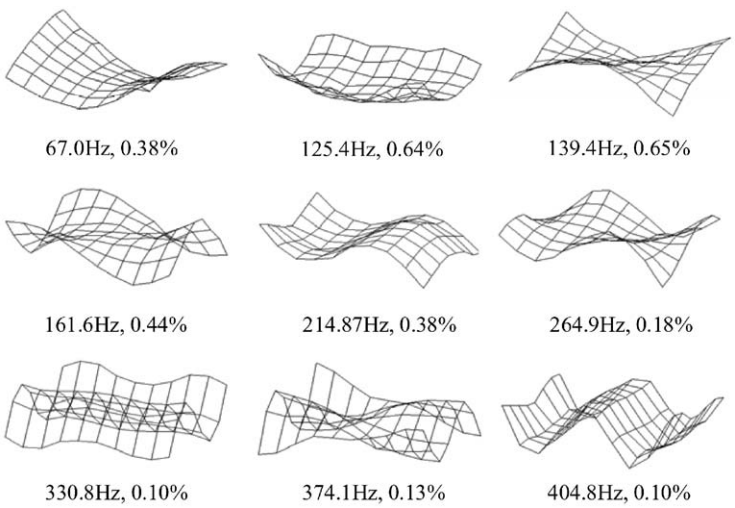

Fig. 9. Measured mode shapes, natural frequencies, and damping ratios of the free plate.

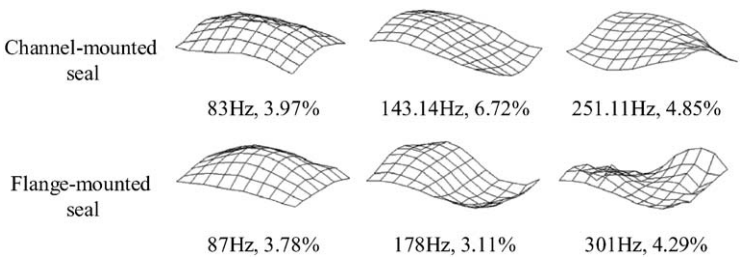

Fig. 10. Measured mode shapes, natural frequencies, and damping ratios of the plate supported by two different viscoelastic supports—channel- and flange-mounted seals.

Table 1
Measured modal properties of the plate

Type of supports	Modal parameter	1×1	2×1	2×2
Flange-mounted seals	Natural frequency (Hz)	87 (87)	178 (179)	301 (289)
	Damping ratio (%)	3.78 (2.24)	3.11 (3.37)	4.29 (5.15)
Channel-mounted seals	Natural frequency (Hz)	83 (82)	143 (162)	251 (249)
	Damping ratio (%)	3.97 (3.98)	6.72 (5.76)	4.85 (8.10)

Calculated modal properties in parenthesis.

systems, the damping ratios were much higher, between 3% and 6%. Obviously, the rubber seals absorb energy and add a significant amount of modal damping to the plate. Consequently, the resolution of closely spaced modes becomes difficult. Only the three modes shown in Fig. 10 could be confidently identified for the seal-supported plate in the 0–500 Hz range. For all three modes, the natural frequency of the plate supported by the flange-mounted seals was higher than that of the plate supported by the channel-mounted seals.

Table 1 shows the comparison between the measured modal parameters and the estimated values. In order to estimate the modal parameters, the Rayleigh–Ritz method [11] was used. The energy loss due to material damping within the plate itself was neglected because the experimental modal analysis suggested that most of the energy dissipation was produced by the sealing systems. Since the mode shapes measured for the seal-supported plates, as shown in Fig. 10, were very close to those of the plates supported by translational springs only, the rotational stiffness values of the seals were neglected. Thus, the viscoelastic properties of the sealing systems were modelled as translational springs with complex stiffness at the four edges of the plate, and assumed to be frequency independent. The stiffness of the seal has a strong influence on the natural frequencies of the plate, and the loss factor on the modal damping ratio. These two parameters were adjusted in the Rayleigh–Ritz method to match the measured modal properties of the plate, and the results are shown in Table 1. A translational spring with complex stiffness, $\hat{S}_t = 2.2 \times (1 + \mathrm{i}0.25)$ MPa was used to approximate the flange-mounted seal and $\hat{S}_t = 1.2 \times (1 + \mathrm{i}0.30)$ MPa to approximate the channel-mounted seal.

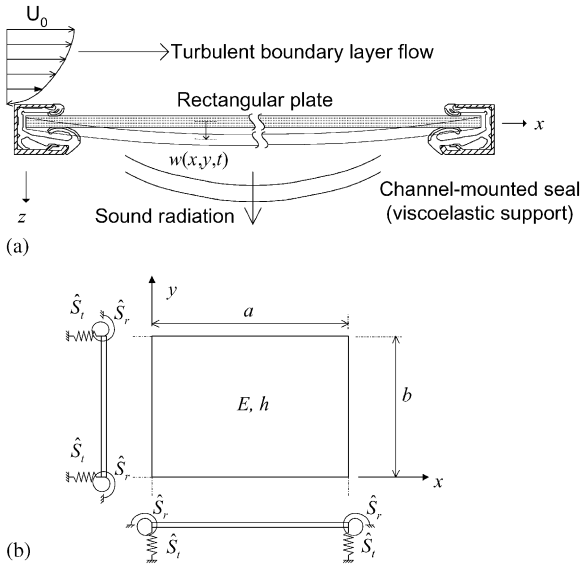

Fig. 11. (a) Sound radiation from the forced vibrations of a seal-supported rectangular plate. (b) Geometry of the rectangular plate and its boundary conditions. The supports are shown from a side view of the plate.

5. Flow-excited response of viscoelasticaly supported plate

5.1. Flow-induced vibration

Fig. 11(a) shows the sound radiation from forced vibrations of a viscoelastically supported plate. This configuration is intended to idealize a seal-supported vehicle side-glass window. Fig. 11(b) shows a schematic of the viscoelastically supported rectangular plate. The numerical model can handle a restraint of the motion of the four edges via translational and rotational springs. Following the results of the mode shapes in Section 4, in the present application of the model to estimate the stiffness of the seal and the flow-induced response, the rotational stiffness of the seal was assumed to be negligibly small.

To calculate the forced vibration response, the frequency response function between a harmonic excitation at one location and the resulting harmonic transverse displacement response at another location was used. With the turbulent flow excitation specified as the cross-spectral density of the wall pressure, the spatially averaged mean square velocity of the plate, v_{av}, is calculated as [11]

$$v_{av}(\omega) = \sum_{j=1}^{N^2} |\omega \hat{H}_j(\omega)|^2 \int_A \int_A \hat{\Psi}_j(\mathbf{s}_1)\hat{\Psi}_j^*(\mathbf{s}_2)\hat{G}_{pp}(\mathbf{s}_1, \mathbf{s}_2, \omega)\, \mathrm{d}\mathbf{s}_1\, \mathrm{d}\mathbf{s}_2, \tag{2}$$

where $\hat{H}_j$ are the frequency response functions for the generalized co-ordinate, A is the plate surface, $\mathbf{s}_1$ and $\mathbf{s}_2$ are the position vectors, and $\hat{\Psi}_j$ are the modal shape functions. The Rayleigh–Ritz method was used applying beam functions as the trial functions to calculate the modal shape functions and the natural frequencies. Details of the Rayleigh–Ritz method and the calculation of flow-induced vibration when the Corcos model is used as cross-spectral density (Eq. (1)) were described in Ref. [11].

5.2. Sound radiation from a viscoelastically supported plate

Assuming a baffled plate mounted on an infinite rigid plane surface, the radiated sound power was calculated as the integral of the far-field acoustic intensity over a hemisphere surrounding the plate as described in Ref. [12]. When the Corcos model is used as cross-spectral density, the radiated sound power may be calculated, assuming inter-modal terms are negligible, using

$$W_r = \frac{\rho_a cab}{2} \sum_{j=1}^{N^2} \sigma_j(\omega)|\omega \hat{H}_j(\omega)|^2 \int_A \int_A \hat{\Psi}_j(\mathbf{s}_1)\hat{\Psi}_j^*(\mathbf{s}_2)\hat{G}_{pp}(\mathbf{s}_1, \mathbf{s}_2, \omega)\, d\mathbf{s}_1\, d\mathbf{s}_2, \tag{3}$$

where σ_j is the radiation efficiency of the jth mode, ρ_a is the density of air, and c is the speed of sound in air. The numerical procedures to calculate the radiation efficiency, σ_j, were described in Ref. [12].

6. Results

6.1. Velocity response of the plate

The plate transverse velocity spectra were measured using the laser vibrometer. Typical results are shown in Figs. 12(a) and (b), where the velocity level in the 160 Hz one-third octave band is plotted as a function of position for the plates supported by two different sealing systems. The center frequency of this band corresponds approximately to the natural frequency of the 2×1 mode of the plate (Table 1). The velocity distribution (Fig. 12) exhibited the main characteristics of the 2×1 mode very clearly. This frequency was selected for presentation because the damping ratio of the plate with the channel-mounted seals was almost twice that of the plate with the flange-mounted seals for the 2×1 mode, and the associated natural frequencies were significantly different. For a given excitation level, the velocity response of the plate was much larger for the flange-mounted seals (3.11% damping ratio) than for the channel-mounted seals (6.72% damping ratio) in the 160 Hz one-third octave band.

Fig. 13 shows measured spatially averaged velocity levels. The velocity levels reflect the characteristics of the wall pressure spectra—large low-frequency fluctuations (Fig. 6). The results of the model predictions are included too. The measured wall pressure spectra and the Corcos model were used as the distributed excitation over the plate in the predictions.

For the plate excited by the reattached flow, the velocity signals were uncorrupted only up to 500 Hz due to the limited dynamic range of the laser vibrometer used in the experiments. The predicted velocity spectra were greater than the measured values around the fundamental frequency region (which is around 87 Hz). The underestimated damping ratio caused an overestimation of the velocity response near the fundamental frequency region. In frequency regions away from this region, the difference was less than 3 dB. For the separated/reattached flow, the measured wall pressure spectra at the leading edge of the plate were used as the excitation to predict the velocity response. Trends are very similar to the results for the plate excited by the reattached flow except the difference in the level of the velocity response.

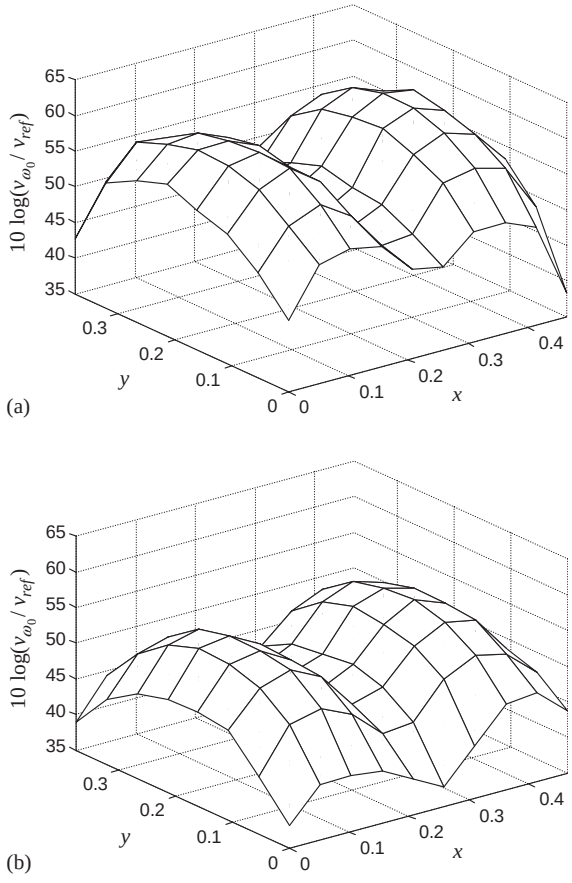

Fig. 12. Spatial distribution of velocity level in the 160 Hz one-third octave band for the plate supported by two different sealing systems: (a) flange-mounted seals and (b) channel-mounted seals.

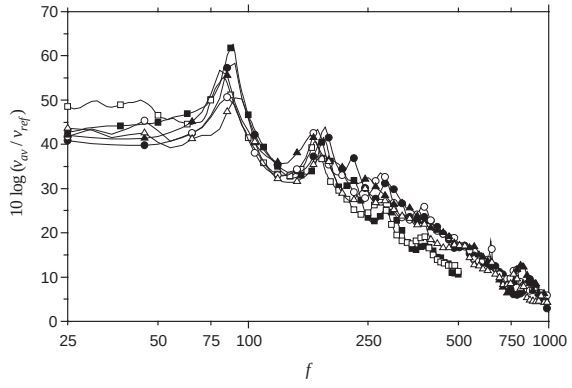

Fig. 13. Spatially averaged velocity spectral density of the plate for three different cases of turbulent flows and sealing systems: (1) the reattached flow and the flange-mounted seals, —□— , measured; —■—, calculated; (2) the separated/reattached flow and the flange-mounted seals, —○— , measured; —●—, calculated; (3) the separated/reattached flow and the channel-mounted seals —△— , measured; —▲—, calculated. $U_0 = 43.6\,\mathrm{m/s}$.

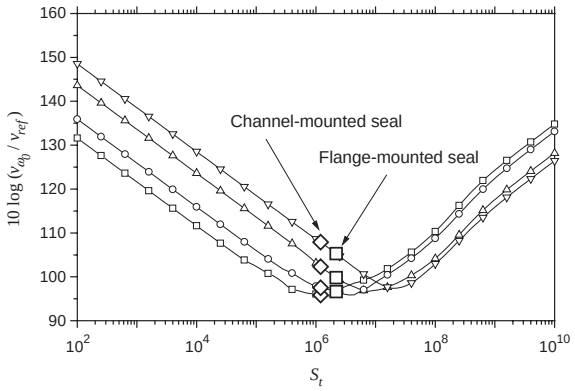

Fig. 14. Effects of the translational stiffness on spatially averaged velocity level in octave bands. $\hat{S}_t = S_t(1 + i0.15)$, center frequencies: —□— , 250 Hz; —○— , 500 Hz; —△— , 1000 Hz; —▽— , 2000 Hz.

From a comparison between the velocity response of the plates supported by the flange-mounted seals and the channel-mounted seals, Fig. 13, the differences were less than 3 dB in general. The estimated seal stiffness of the channel-mounted seals was approximately 54% than that of the flange-mounted seals. Although considerable differences were found at low frequencies (near the fundamental frequency of the plate), the overall response of the plate was not sensitive to the seal mechanical properties for the flange-mounted and channel-mounted seals investigated here.

A more systematic investigation of the effects of translational stiffness on the plate vibration response was performed in Ref. [12]. Fig. 14 shows the variation of the velocity response with the translational stiffness, S_t from which the optimal translational stiffness was determined. The delta function was used as a correlation function for the distributed pressure fields. The results for octave bands centered at 250, 500, 1000 and 2000 Hz are shown together with the measured translational stiffness of the sealing systems used in the experiments, and the corresponding spatially averaged mean square velocities. Although the loss factor used in this simulation is different from the measured values in Section 4, the dependence of the optimal support stiffness on the loss factor was negligible if the loss factor is less than 0.4 [12]. The stiffness for both sealing systems is near the optimal translational stiffness especially for the 250 Hz octave band. The sensitivity to variations in support stiffness around the optimal values was weak, which explains the trends observed in the experimental data.

6.2. Sound radiation

The radiated sound power was calculated using Eq. (3). Assuming the radiated acoustic pressure to be uniformly distributed over a semi-spherical surface, the radiated sound power was calculated from the measured acoustic pressure at a single point in the receiving enclosure. The predictions from Eq. (3), along with the measured sound power are plotted in Fig. 15. The noise of the wind tunnel exceeded the radiated sound pressure at low frequencies (below 80 Hz). The sound measurements were corrupted by noise from the wind tunnel. Several factors may have

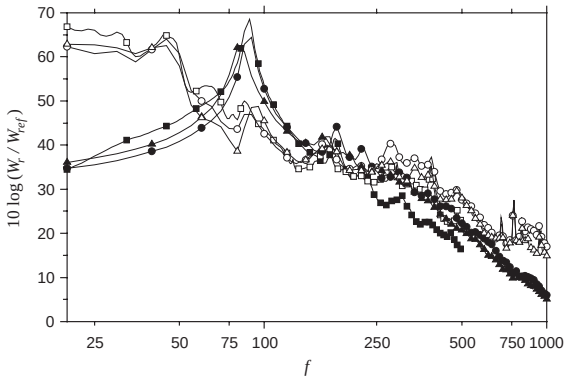

Fig. 15. Sound power spectra radiated from the plate for three different cases of turbulent flows and sealing systems. (1) The reattached flow and the flange-mounted seals: —□—, measured; —■—, calculated. (2) The separated/reattached flow and the flange-mounted seals: —○—, measured; —●—, calculated. (3) The separated/reattached flow and the channel-mounted seals: —△—, measured; —▲—, calculated. $U_0 = 43.6\,\mathrm{m/s}$.

contributed to the discrepancies between measurements and predictions. The sound absorbing treatment of the cavity was not perfect, thus cavity resonance inside the receiving enclosure may have played a role at low frequencies. Similar to the velocity response, the differences in the radiated sound power between the plates supported by the flange-mounted seals and the channel-mounted seals were not significant.

7. Conclusions

The vibration response and the sound radiated from a flow-excited viscoelastically supported rectangular plate were investigated in a controlled laboratory setup. It was found that the viscoelastic supports—actual vehicle seals—significantly influenced the vibro-acoustic properties of the supported plate. The seals were found to add a considerable amount of damping to the system, and this suggested that dissipation of vibration energy occurs mostly at the supports rather than within the seal-supported plate itself.

Two different types of seals were tested—channel-mounted and flange-mounted seals. The wall pressure on the plate surface was measured to determine the excitation from the wind flow. Considerable differences in the velocity response of the plate supported by two different sealing systems were observed near the fundamental frequency. Overall, within the frequency range of interest, the two sealing systems produced similar flow-induced vibration responses and sound power radiations. The investigation confirmed that the properties of both sealing systems were close to the optimal stiffness values that minimize the velocity response of the plate.

The damping treatments at the boundaries increase the system damping ratios and reduce the aerodynamic noise generated from the window significantly. The presented experimental procedures together with the analytical methods can be used as systematic methods to test the performance of seals as damping treatments and to guide the design of sealing systems.

Acknowledgements

The authors express their thanks to Ford Motor Company and Advanced Elastomer Systems for financial support and their guidance. The contribution of the Herrick Laboratories Technical staff is also gratefully acknowledged. An earlier, different version of this paper has been published before in a different format [15].

Appendix A. Nomenclature

c speed of sound in air (m/s)
f frequency (Hz)
$\hat{G}_{pp}$ wall pressure cross-spectral density (Pa^2/Hz)
h_f fence height (m)
$\hat{H}_j$ frequency response functions in terms of generalized co-ordinates
p_{ref} reference pressure, 20 μPa
$\hat{S}_t$ complex stiffness of translational spring (Pa)
U_c convection velocity (m/s)
U_o free stream flow velocity (m/s)
v_{av} spatially averaged mean square velocity of plate (m^2/s^2/Hz)
v_{ref} reference mean square velocity, 10^{-12} (m^2/s^2)
v_{ω_0} spatially averaged mean square velocity in octave bands (m^2/s^2)
W_r radiated sound power (W/Hz)
W_{ref} reference power, 10^{-12} (W)
x_f distance from fence in x direction (m)
γ_x, γ_y decay rate in x and y directions
$\hat{\Psi}_{mn}$ modal shape functions of plate
ξ_x, ξ_y separation distance in x and y directions (m)
ρ_a density of air (kg/m^3)
σ_j radiation efficiency of the jth mode
Φ_p pressure spectral density (Pa^2/Hz)
ω circular frequency (rad/s)

References

[1] A.R. George, J.R. Callister, Aerodynamic noise of ground vehicles, SAE General Aviation Meeting, Wichita, KS, Paper No. 911027, 1991, pp. 1–28.
[2] G.S. Strumolo, The wind noise modeler, *Proceedings of the 1997 SAE Noise & Vibration Conference*, Traverse City, MI, Paper No. 971921, 1997, pp. 417–425.
[3] S.F. Wu, G. Wu, M.M. Puskarz, M.E. Gleason, Noise transmission through a vehicle side window due to turbulent boundary layer excitation, *Journal of Vibration and Acoustics* 119 (1997) 557–562.
[4] W.B. Coney, J.Y. Her, J.A. Moore, Characterization of the wind noise loading of production automobile greenhouse surfaces, *Fourth International Symposium on Fluid–Structure Interactions, Aeroelasticity, Flow–induced Vibration and Noise*, Vol. 1, Dallas, TX, 1997, pp. 411–418.
[5] W.K. Blake, *Mechanics of Flow-induced Sound and Vibration, Volumes I &II*, Academic Press, New York, 1986.

[6] T.M. Farabee, M.J. Casarella, Effects of surface irregularity on turbulent boundary layer wall pressure fluctuations, *Journal of Vibration, Acoustics, Stress, and Reliability in Design* 106 (1984) 343–350.
[7] T.M. Farabee, M.J. Casarella, Measurements of fluctuating wall pressure for separated, reattached boundary-layer flows, *Journal of Vibration, Acoustics, Stress and Reliability in Design* 108 (1986) 301–307.
[8] W.A. Strawderman, R.S. Brand, Turbulent-flow-excited vibration of a simply supported, rectangular flat plate, *Journal of the Acoustical Society of America* 45 (1968) 177–192.
[9] G.M. Corcos, Resolution of pressure in turbulence, *Journal of the Acoustical Society of America* 35 (1963) 192–199.
[10] F. Han, R.J. Bernard, L.G. Mongeau, Prediction of flow-induced structural vibration and sound radiation using energy flow analysis, *Journal of Sound and Vibration* 227 (1999) 685–709.
[11] J. Park, L. Mongeau, T. Siegmund, Analysis of the flow-induced vibrations of viscoelastically supported rectangular plates, *Journal of Sound and Vibration* 261 (2003) 225–245.
[12] J. Park, L. Mongeau, T. Siegmund, Influence of support properties on the sound radiated from the vibrations of rectangular plates, *Journal of Sound and Vibration* 264 (2003) 775–794.
[13] D.V. Brown, L. Mongeau, The design, construction, and validation of a small, low-speed, quiet wind tunnel with application to noise from the flow over a cavity, *Ray W. Herrick Laboratories, Purdue University, Internal Report No. 204*, 1995.
[14] T.F. Brooks, T.H. Hodgson, Trailing edge noise prediction from measured surface pressures, *Journal of Sound and Vibration* 78 (1981) 69–117.
[15] J. Park, T. Siegmund, L. Mongeau, Sound radiation from a flow-excited rectangular plate with viscoelastic supports, *Proceedings of 2001 ASME International Mechanical Engineering Congress and Exposition*, Paper No. IMECE2001/NCA-23508, New York, 2001.